

GEOMETRIC CALIBRATION OF THERMOGRAPHIC CAMERAS

Thomas Luhmann* Julia Ohm, Johannes Piechel, Thorsten Roelfs

Institute for Applied Photogrammetry and Geoinformatics, Jade University of Applied Sciences Oldenburg, Ofener Str.
 16-19, D-26121 Oldenburg, Germany (thomas.luhmann@jade-hs.de)

Commission V, WG V/5

KEY WORDS: Thermography, Thermal Imaging, Calibration, Accuracy, Application

ABSTRACT:

The paper gives an overview of thermal imaging sensors for photogrammetric close-range applications. In particular, it presents results of the geometric calibration of thermographic cameras as they are used for building inspection and material testing. Two different test fields have been designed providing point targets that are visible in the thermal spectral band of the cameras.

Five different cameras have been investigated. Four of them have solid state sensors with pixel sizes between 25 and 40 μm . One camera is working in scanning mode. The lenses for thermographic cameras are made of Germanium. Conventional imaging configurations (typically 20 images) have been used for camera calibration. Standard parameters for principal distance, principal point, radial distortion, decentring distortion, affinity and shear have been introduced into the self-calibrating bundle adjustment. All measured points are introduced as weighted control points. Image coordinates have been measured either in the professional software package AICON 3D Studio (ellipse operators), or in the IAPG software system Stereomess (least-squares template matching).

The calibration results differ significantly from camera to camera. All lenses show relatively large decentring distortion and deviations from orthogonality of the image coordinate axes. Using the plane test field with lamps, the average image precision is $3/10^{\text{th}}$ of a pixel while the 3D test field with circular reflecting targets results in imaging errors of $1/20^{\text{th}}$ pixel.

1. CAMERA TECHNOLOGY

1.1 Physical background

Thermographic cameras are widely used in the fields of material testing, quality control and building monitoring. In all of these cases the radiometric information about temperature distribution is of major interest. Geometric applications are still rare, hence camera developers and suppliers still show little interest in photogrammetric techniques. However, with increasing resolution of thermographic cameras the geometric processing of the image data will become more important.

The specific spectral emission M_λ of an object is defined by Planck's emission law as a function of absolute temperature and wavelength (Wolfe & Zissis, 1985):

$$M_\lambda \left[\frac{W}{\text{cm}^2 \cdot \mu\text{m}} \right] = \frac{c_1}{\lambda^5} \frac{1}{\exp\left(\frac{c_2}{\lambda \cdot T}\right) - 1} \quad (1)$$

where

- c_1 : 1. emission constant = $3,7418 \cdot 10^4 \text{ W} \cdot \text{cm}^{-2} \cdot \mu\text{m}^4$
- c_2 : 2. emission constant = $1,4388 \cdot 10^4 \text{ K} \cdot \mu\text{m}$
- T : absolute temperature [K]
- λ : wave length [μm]

Fig. 1 shows the well known diagram of specific spectral emission for different absolute temperatures according to equation (1). It makes clear that only objects with a temperature of more than about 1000 K are emitting electro-magnetic radiation visible for the human eye or conventional cameras.

The maximum of the specific emission is described by Wien's displacement law:

$$\lambda_{\text{max}} = \frac{2897.8}{T} \quad (2)$$

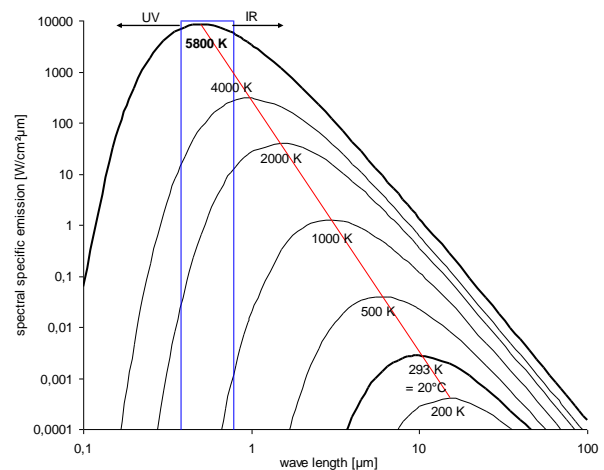


Fig. 1: Spectral specific emission

In equation (2) the value 2897.8 is denoted as the Wien displacement constant. The formula states that the wavelength of maximum emission of an object is a reciprocal function of the temperature, hence higher temperatures yield lower wave lengths (Dereniak & Boreman, 1996). As an example, the sun has an average temperature of about 5800 K, the resulting wavelength is 0.5 μm , thus in the yellow band of the visible

light spectrum. As a second example, an object of 20°C (=293 K), the resulting wavelength is about 10 µm.

Consequently thermographic cameras need imaging sensors that are sensitive to wavelengths usually between 2.5 and 15 µm. Depending on the detector technology (see section 1.2) temperatures between -30 and +400°C can be detected by common thermographic cameras.

The geometric resolution of imaging devices is limited by diffraction. The diameter of the Airy disk d depends on the aperture (f-number k) and the wavelength:

$$d = 2.44 \cdot \lambda k \quad (3)$$

As an example, geometric resolution at a wavelength of $\lambda=10 \mu\text{m}$ at f-number $k=2$ is limited to about 48 µm. Equation (3) makes clear that the pixel sizes of thermal sensors can be much larger than for standard RGB cameras. In fact most thermal imaging sensors provide pixel sizes between 30 and 50 µm.

1.2 Detectors

Sensors for thermal cameras are either quantum detectors or thermal detectors (Nolting, 2007). Quantum detectors are based on the inner photo-electric effect where electrons are set free between two layers of a semi-conductor device. Quantum detectors are very sensitive ($\pm 0.01 \text{ K}$) and fast, but need an external cooling system (Peltier or Sterling elements) (Fouad & Richter, 2008).

Thermal detectors use the effect that a temperature change of the detector element leads to a change of the electrical properties of the detector, e.g. resistance or charges (Bauer, 2008). These changes can be measured and transformed into intensity values. Thermal detectors are available in different designs such as pyro-electric detectors or bolometers. Thermal detectors are less sensitive ($\pm 0.1 \text{ K}$) and slower than quantum detectors, but do not need any cooling elements. Hence they are less expensive and usually applied for applications like building monitoring.

As state-of-the-art typical thermal array sensors are available with 320 x 240 pixels up to 640 x 320 pixels. Sensor sizes then yield about up to 20-30 mm in each direction. Newest camera developments show pixel numbers of up to 1280 x 960

In principle thermographic cameras built on solid state sensors can be handled as standard photogrammetric cameras. Due to the longer wavelengths the lenses of thermographic cameras are made of Germanium which makes them extremely expensive. These lenses are optimized for radiometric resolution, thus geometric precision or minimal distortion are of less interest.

2. TEST FIELDS FOR CALIBRATION

2.1 Plane testfield with lamps

A plane testfield provided by the University of Dessau consists of 57 small lamps that warm up when switched on. The dimension of the wooden plate is about 1000 mm x 1000 mm

(Fig. 2). The positions of the lamps have been measured by a theodolite system with an accuracy of about 0.2 mm.



Fig. 2: Plane testfield with active lamps

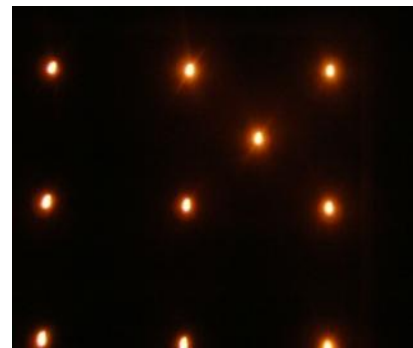


Fig. 3: Burning target lamps

The quality of the active targets is quite poor (Fig. 3). It is obvious that the centre of the targets lamps can not be measured with a precision as usually provided by photogrammetric targets. In addition, camera calibration with plane testfields is less accurate and less significant compared to 3D testfields.

2.2 Spatial testfield with coded targets

Since the plane testfield is not ideal for camera calibration a new design was investigated. The basic idea was to create targets that generate sufficient image contrast in the thermal spectrum. In addition, the new testfield should be mobile, easy to calibrate and cost effective without any need for artificial heating of targets.

Several experiments have been carried out in order to find a suitable combination of target material and lighting. Finally, the effect of cold sky temperature has been used to create a testfield design that fulfils the above mentioned specifications.

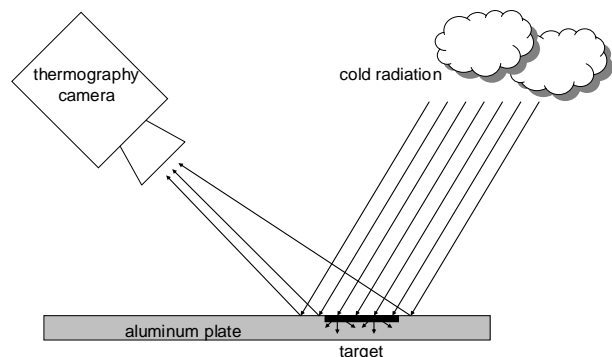


Fig. 4: Target absorption of cold sky radiation

Fig. 4 shows the reflectance principle. Assuming diffuse reflectance of the metal testfield plate the cold temperature of space reflects on the metal surface. Since the target is made of self-adhesive foil it only emits radiation relating to its own temperature. With this principle the acquired image displays a strong contrast because targets appear bright while the surrounding areas appear dark (Fig. 5).

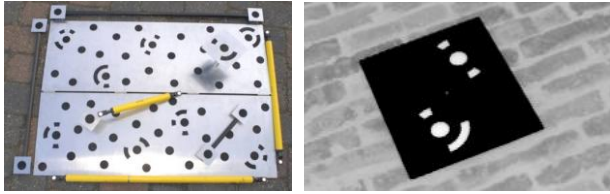


Fig. 5: Testfield and thermal image of targets

Based on the new design of target points a mobile testfield has been built. It consists of about 17 coded targets and 35 uncoded targets, and additional height points. Additional scale bars with the same type of targets can be mounted onto the testfield. Due to the target design a conventional photogrammetric calibration of the testfield is possible which yields control points coordinates.

The size of the testfield is about 1000 mm x 700 mm x 200 mm. The accuracy of control points after measurement with a high-resolution digital camera and bundle adjustment is estimated to 8µm in object space.

3. CALIBRATION RESULTS

3.1 Cameras

Table 1 summarizes the technical data of four thermographic cameras that are included in the test. A fifth camera works with a rotation mirror device for image scanning. Due to the instable mechanical rotation and the non-perspective imaging model this camera has been eliminated from further tests for the time being.

The investigated cameras (see Fig. 6) show more or less similar technical data. However, due to the different detector elements their performance differs as well as their market prices.

	FLIR InfraCam	Testo 880-3	FLIR B200	InfraTec VarioCam
pixels	240 x 240	320 x 240	320 x 240	384 x 288
pixel size	0.025 mm	0.035 mm	0.04 mm	0.035 mm
focal length	10 mm	10 mm	18 mm	11 mm
thermal resolution	±0.2°C	< 0.3°C	±0.08°C	0.08 - 0.05°C
price [€]	ca. 4000	ca. 6500	ca. 9000	ca. 19000

Table 1: Investigated thermographic cameras

3.2 Calibration results

Each camera was calibrated according to standard imaging configurations (Luhmann et al., 2006) with about 20 multi-convergent images. Both testfields as explained in section 2 have been used (Fig. 7). The plane testfield with burning lamps

can be measured inside a lab while the reflective 3D testfield has to be used in open air.



Fig. 6: Investigated thermographic cameras

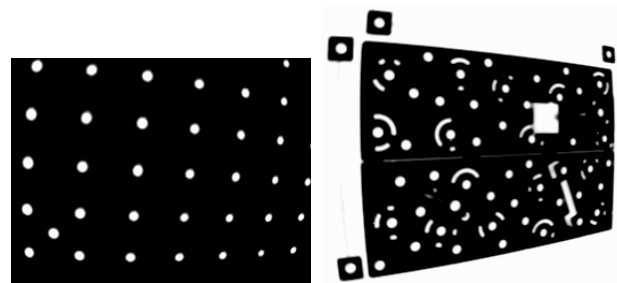


Fig. 7: Thermal images acquired from plane testfield (left) and spatial testfield (right)

Image measurement and bundle adjustment were performed with AICON 3D Studio. The calibration results, derived from the spatial testfield, are listed in Tables 2-5. The plane testfield leads to similar results. However the precision of the estimated parameters is reduced and therefore they are not listed here.

parameter	value	standard dev.
principal distance c	-13.8971 mm	0.0104
principal point x' ₀	-0.2940 mm	0.0188
principal point y' ₀	-0.3430 mm	0.0197
radial-sym. distortion A ₁	-2.80·10 ⁻³	1.33·10 ⁻⁴
radial-sym. distortion A ₂	6.86·10 ⁻⁷	2.03·10 ⁻⁵
radial-sym. distortion A ₃	7.76·10 ⁻⁷	9.52·10 ⁻⁷
decentering distortion B ₁	1.91·10 ⁻⁵	2.10·10 ⁻⁵
decentering distortion B ₂	-2.69·10 ⁻⁵	2.25·10 ⁻⁵
affinity C ₁	6.84·10 ⁻⁴	1.99·10 ⁻⁴
shear C ₂	-2.22·10 ⁻⁴	2.21·10 ⁻⁴

Table 2: Calibrated camera parameters (FLIR InfraCam)

parameter	value	standard dev.
principal distance c	-19.9373 mm	0.0297
principal point x'_0	-0.1571 mm	0.0524
principal point y'_0	0.2110 mm	0.0376
radial-sym. distortion A_1	$-7.25 \cdot 10^{-4}$	$1.20 \cdot 10^{-4}$
radial-sym. distortion A_2	$-9.59 \cdot 10^{-6}$	$7.19 \cdot 10^{-6}$
radial-sym. distortion A_3	$1.86 \cdot 10^{-7}$	$1.28 \cdot 10^{-7}$
decentering distortion B_1	$5.12 \cdot 10^{-5}$	$1.22 \cdot 10^{-5}$
decentering distortion B_2	$-3.51 \cdot 10^{-5}$	$1.72 \cdot 10^{-5}$
affinity C_1	$7.50 \cdot 10^{-4}$	$3.16 \cdot 10^{-4}$
shear C_2	$8.18 \cdot 10^{-4}$	$2.96 \cdot 10^{-4}$

Table 3: Calibrated camera parameters (Testo 880-3)

parameter	value	standard dev.
principal distance c	-36.9443 mm	0.0223
principal point x'_0	1.4445 mm	0.0574
principal point y'_0	-1.8332 mm	0.0420
radial-sym. distortion A_1	$-2.69 \cdot 10^{-4}$	$1.94 \cdot 10^{-5}$
radial-sym. distortion A_2	$-7.47 \cdot 10^{-7}$	$6.94 \cdot 10^{-7}$
radial-sym. distortion A_3	$2.79 \cdot 10^{-9}$	$7.40 \cdot 10^{-9}$
decentering distortion B_1	$-2.78 \cdot 10^{-4}$	$5.21 \cdot 10^{-6}$
decentering distortion B_2	$-1.72 \cdot 10^{-5}$	$6.18 \cdot 10^{-6}$
affinity C_1	$-6.11 \cdot 10^{-4}$	$2.60 \cdot 10^{-4}$
shear C_2	$-8.66 \cdot 10^{-4}$	$2.61 \cdot 10^{-4}$

Table 4: Calibrated camera parameters (FLIR B200)

parameter	value	standard dev.
principal distance c	-11.8188 mm	0.0014
principal point x'_0	0.0201 mm	0.0013
principal point y'_0	0.1400 mm	0.0012
radial-sym. distortion A_1	$-2.41 \cdot 10^{-3}$	$4.93 \cdot 10^{-6}$
radial-sym. distortion A_2	$8.76 \cdot 10^{-6}$	$1.83 \cdot 10^{-7}$
radial-sym. distortion A_3	$-2.67 \cdot 10^{-8}$	$2.05 \cdot 10^{-9}$
decentering distortion B_1	$5.23 \cdot 10^{-5}$	$1.11 \cdot 10^{-6}$
decentering distortion B_2	$-1.29 \cdot 10^{-5}$	$1.14 \cdot 10^{-6}$
affinity C_1	$-7.79 \cdot 10^{-5}$	$2.47 \cdot 10^{-5}$
shear C_2	$1.85 \cdot 10^{-4}$	$1.91 \cdot 10^{-5}$

Table 5: Calibrated camera parameters (InfraTec VarioCam)

The cameras FLIR InfraCam, Testo 880-3 and FLIR B200 show relatively weak results in terms of image measurement precision and standard deviations of principal point and principal distance. Compared to the given focal length (as taken from data sheets) the principal distance differs significantly. In the case of the FLIR B200 the principal point shift amounts to more than 1.4 mm, which corresponds to more than 35 pixels. All cameras show relatively large radial distortion values as depicted in Fig. 8.

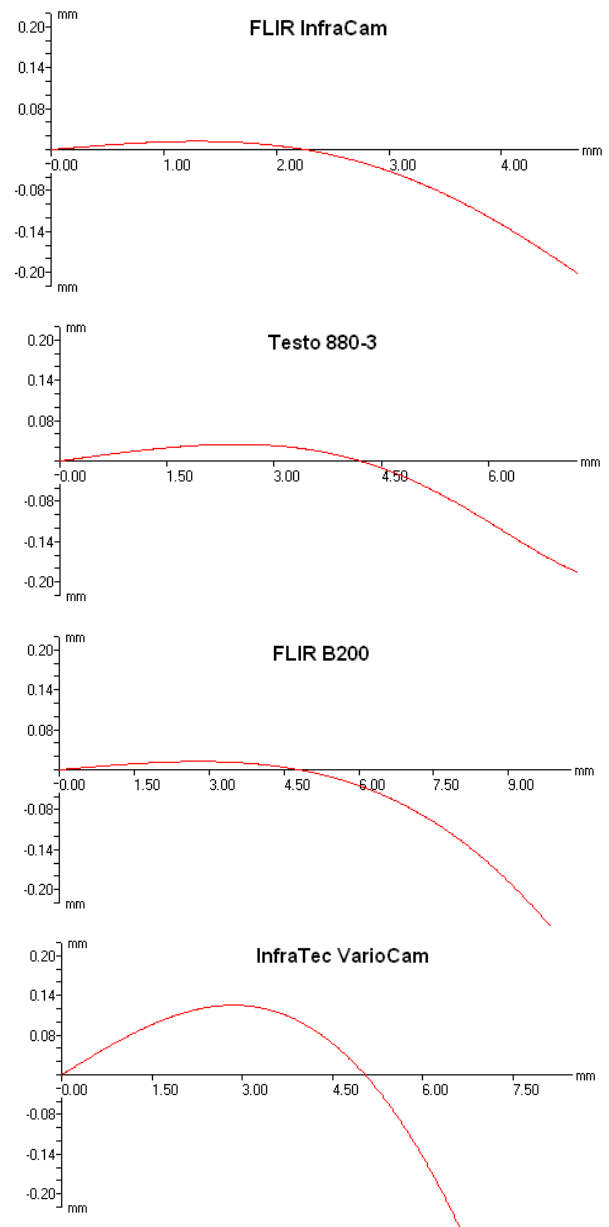


Fig. 8: Distortion curves

The camera InfraTec VarioCam yields the best results in terms of precision of the estimated parameters. The precision of image point measurement lies in the order of 1 μ m or 1/30th of a pixel. For this camera the principal point shows moderate shift with respect to the centre of the image, and the principal distance is close to the given focal length.

The resulting precision in object space is estimated by RMS values of adjusted object coordinates. External reference values, for instance calibrated lengths, are not available in this test. Table 6 summarizes the results in object space. As expected from the calibration quality discussed above, the three cameras FLIR InfraCam, Testo 880-3 and FLIR B200 yield RMS values (1 sigma) of about 0.11 to 0.24 mm, which corresponds to about 1:6000 of the largest object diameter. The Infrectec VarioCam results in RMS values of 0.03 to 0.06 mm, corresponding to about 1:20000.

camera	X	Y	Z
FLIR InfraCam	0.110 mm	0.118 mm	0.143 mm
Testo 880-3	0.137 mm	0.160 mm	0.236 mm
FLIR B200	0.148 mm	0.185 mm	0.145 mm
Infratec VarioCam	0.038 mm	0.029 mm	0.062 mm

Table 6: RMS 1-sigma values of object coordinates

4. APPLICATIONS

If thermographic cameras are calibrated in terms of the geometric imaging model they can be used for a variety of practical applications (Kaplan, 2007).

4.1 2D processing

For two-dimensional purposes thermal images can be resampled to distortion-free images. As an example Fig. 9 shows the original thermal image taken with the InfraTec VarioCam camera. Radial distortion is clearly visible. Fig. 10 shows the same image after correction of distortion. Geometrically corrected thermographic imagery can be used as thermal orthophotos, maps or mosaics, or as precise texture images for 3D city or building models.

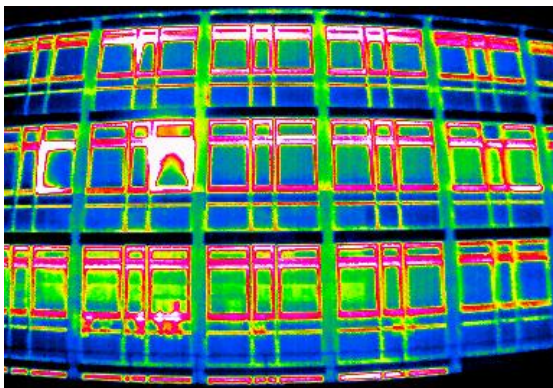


Fig. 9: Original thermal image (camera: InfraTec VarioCam)



Fig. 10: Distortion-free thermal image

It has to be pointed out that modified thermographic images often can not be processed by those software packages that are provided with a specific camera system. As an example, the FLIR software package allows for post-processing of original FLIR imagery, e.g. changing temperature scales or colour tables.

4.2 3D processing

Three-dimensional applications are also possible since thermographic images can be used in the same way as conventional photogrammetric images. However, in this case it is required to match corresponding points.

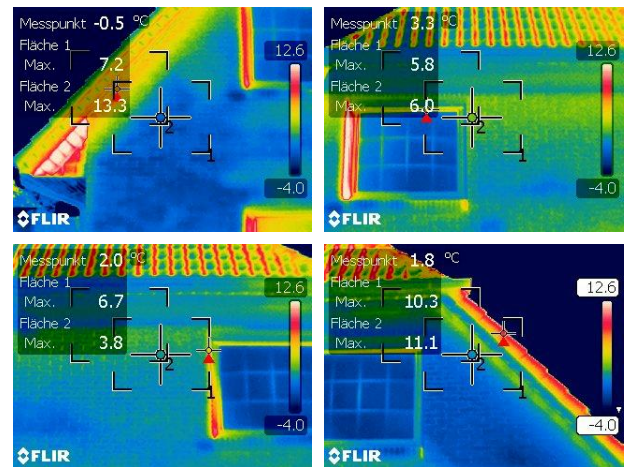


Fig. 11: Multi-image thermography

Fig. 11 shows an example of four overlapping thermographic images taken within a few minutes without changing the camera settings. It is obvious that the thermal emission of the building wall does not behave as a diffuse Lambert reflector. A number of identical object areas are displayed in different colours (temperatures).

Future investigations will concentrate on 3D modelling with thermographic imagery under consideration of radiometric object models.

4.3 Pan sharpening

If a high resolution panchromatic or RGB image is available in addition to a (low resolution) thermal image it is possible to apply pan-sharpening. Both image sources have to be registered (rectified) to the same geometric reference system.

Fig. 12 shows the principle image data flow for thermal pan-sharpening as it has been applied to the images shown below.

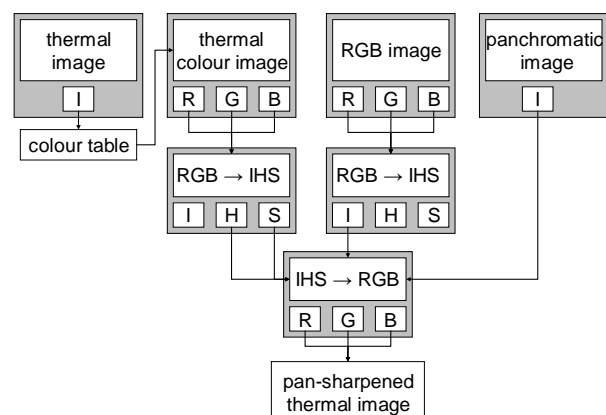


Fig. 12: Image data flow for thermal pan-sharpening

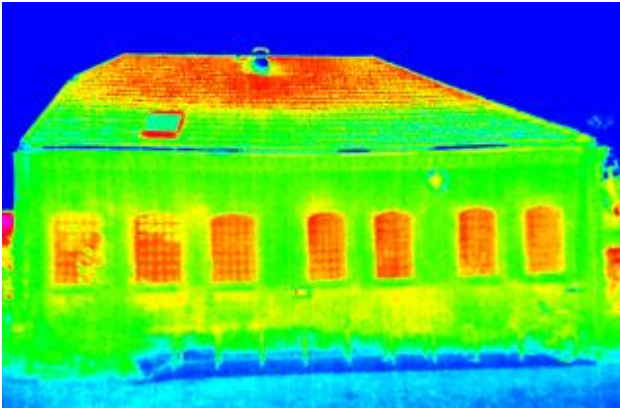


Fig. 13: Original thermal image

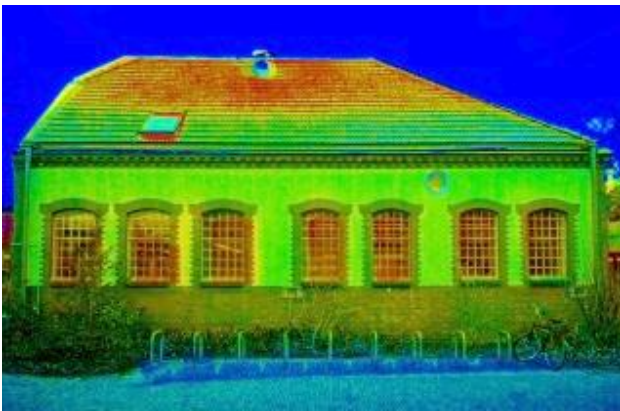


Fig. 14: Example of thermal pan-sharpening

As an example, Fig. 13 shows an original thermal image of a building façade. Fig. 14 displays the result of pan-sharpening using a high-resolution digital image taken with a Nikon D2x camera. In contrast to standard methods in remote sensing (e.g. Toet et al., 1989; Ehlers et al., 2009), applying pan-sharpening to non-planar objects in close-range photogrammetry either requires identical perspectives for each image source, or given 3D object models and full orientation parameters of each image. The example above still shows remaining geometric errors at the back parts of the roof since only a 2D rectification approach has been used.

It should be noted that the colours will change by this processing and an attribution of temperature levels in a following step might lead to erroneous values in small structures. However, the method of pan-sharpening is quite suitable for presentation purposes of thermographic inspections in order to illustrate details of the object.

5. SUMMARY

We have investigated the performance of thermographic cameras with respect to their geometric image model. Standard procedures for camera calibration can be applied to close-range thermal imagery if the cameras consist of array imaging sensors. In addition, the observed object must provide target points that are visible in the thermal spectrum. For this purpose a new testfield has been designed that uses the cold temperature from sky in order to create sufficient image contrast.

The results of camera calibration show that standard thermographic cameras yield high distortion values, and large

shifts of principal point. Only one camera (Infratec VarioCam) provides an accuracy level that is comparable to RGB cameras.

Some example applications are discussed ranging from 2D image modification purposes (rectification, image mosaics) and pan-sharpening approaches up to 3D modeling tasks that uses thermographic imagery in the same way as multi-image photogrammetry. However, the radiometric models of thermal object emission have to be investigated in more detail for a better understanding of the imaging process in convergent cases.

6. REFERENCES

- Bauer, N., (Ed.), 2008. *Handbuch zur Industriellen Bildverarbeitung*. Fraunhofer IRB Verlag, Stuttgart.
- Dereniak, E.L., Boreman, G.D., 1996: *Infrared Detectors and Systems*. Wiley-Interscience, 561 p.
- Ehlers, M., Klonusa, S., Åstrand, P.J., Rosso, P., 2009. Multi-sensor image fusion for pansharpening in remote sensing. *International Journal of Image and Data Fusion*, Vol. 1, No. 1, March 2010, pp. 25–45.
- Fouad, N.A., Richter, T., 2008. *Leitfaden Thermografie im Bauwesen*. Fraunhofer IRB Verlag, Stuttgart, 127 p.
- Kaplan, H., 2007. *Practical Applications of Infrared Thermal Sensing and Image Equipment*. SPIE Publications, 192 p.
- Luhmann, T., Robson, S., Kyle, S., Harley, I., 2006: *Close Range Photogrammetry*. Whittles Publishing, 500 p.
- Nolting, J., 2007. Detektoren für optische Strahlung. *DOZ Optometrie*, 4-2007, pp. 50-56.
- Toet, A., van Ruyven, J.J., Valeton, J.M., 1989: Merging thermal and visual images by a contrast pyramid. *Optical Engineering*, 28(7), pp. 789-792.
- Wolfe, W.L., Zissis, G.J., 1985: *The Infrared Handbook*. Environmental Research Institute of Michigan, 1700 p.